Polymer Journal

AWARD ACCOUNTS
SPSJ Mitsubishi Chemical Award Accounts

Fractal Materials and Their Functional Properties

By Kaoru TSUJII[1,2,*]

Fractal, a mathematical concept, has been utilized to develop some functional materials by the present author and his coworkers. Fractal surfaces show super water- and even oil-repellent property due to their very large surface area. In order to realize the super water-repellent fractal surfaces some waxes (alkylketene dimer and triglycerides) were employed. These waxes interestingly form the fractal surfaces spontaneously. The formation mechanism of the fractal structures on the wax surfaces has been made clear. The waxes which form the fractal surfaces have a meta-stable crystalline phase when solidified from their melts, and then transform to the thermodynamically stable crystal. During this phase transition process, the wax surfaces become fractal. For practical applications in future, durable super water-repellent and highly oil-repellent fractal surfaces have been synthesized by the electrochemical polymerization of an alkylpyrrole and the coating them with a fluorinated alkylsilane-coupling agents. In the final part of this article, the creation of a fractal body, not the surfaces, with a novel template method is mentioned. Such a fractal body is expected to show some interesting and unique functional properties.

KEY WORDS: Fractal / Fractal Surface / Fractal Body / Super Water-repellency / Oil-repellency /

Fractal is a mathematical (geometrical) concept,[1] and has been used for long time as a measure of complexity in the fields of physics, chemistry, industrial technologies, and so on.[2] But the fractal concept has been found by the present author and his coworkers to be also a powerful tool to develop some functional materials. Fractal surfaces, for example, have very large surface area (infinitely large in pure mathematical sense), and this property can be applied to some useful functions. A super water-repellent surface which shows the contact angle of 174° has been obtained by utilizing the above property of the fractal structure.[3,4] Even super oil-repellent surfaces can be synthesized by making the surface fractal.[5,6] A droplet of rape seed oil shows the contact angle of 150°, and rolls around without attachment on this super oil-repellent surface.

In this review article, the author will give some examples of the development of functional materials having the fractal structures, and discuss the following items; i) super water-repellent fractal surfaces of some waxes, ii) formation mechanism of the fractal structures on the wax surfaces, iii) super oil-repellent surfaces of anodically oxidized aluminum, iv) durable super water-repellent and highly oil-repellent surfaces, and v) fractal body created with a novel template method.

WETTABILITY OF FRACTAL SURFACES

Prior to the discussions on the fractal functional materials, the principle of the wetting on the fractal surfaces will be given in this chapter to make the readers understand easily the contents of the following chapters.

Two Factors Governing the Wetting

Figure 1 shows a liquid droplet on a flat solid surface. The wetting can be represented quantitatively by the contact angle θ. We call wettable (repellent) surface when the contact angle is smaller (greater) than 90°. The contact angle is determined by the balance in horizontal direction of three surface and interfacial tensions (γ_S, γ_L, γ_{SL}), where γ_S, γ_L, γ_{SL} are the surface tensions of solid, liquid and interfacial tension between solid and liquid, respectively. This balance among the surface and the interfacial tensions in the horizontal direction is expressed by the well-known Young's equation as follows;[7]

$$\cos\theta = \frac{(\gamma_S - \gamma_{SL})}{\gamma_L}. \quad (1)$$

The wettability of a liquid on a solid surface is governed by one more factor, *i.e.*, the geometrical (surface roughness) factor of the solid surfaces.[8–10] Wenzel suggested that the contact angle θ_r of a liquid droplet placed on a rough solid surface was written as eq (2).[8]

$$\cos\theta_r = \frac{r(\gamma_S - \gamma_{SL})}{\gamma_L} \quad (2)$$

where r is a roughness factor which is defined as the ratio of actual surface area of a rough surface to the geometric projected area. Then, the relationship between θ_r and θ is given by eq (3) combining the eqs (1) and (2).

$$\cos\theta_r = r\cos\theta \quad (3)$$

Eq (3) indicates that the rough surface is more repellent (more wattable) to a liquid when θ is greater (smaller) than 90°,

[1]Nanotechnology Research Center, Research Institute for Electronic Science, Hokkaido University, N-21, W-10, Kita-ku, Sapporo 001-0021, Japan
[2]JST, CREST
*To whom correspondence should be addressed (Tel: +81-45-897-2176, Fax: +81-45-897-2176, E-mail: tsujik@gc4.so-net.ne.jp).

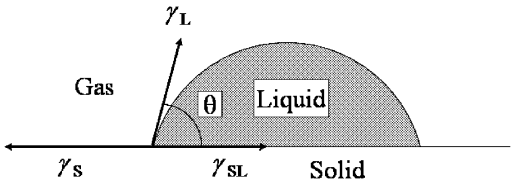

Figure 1. Wettability of a liquid droplet on a solid surface. Contact angle θ is determined by the horizontal balance among the surface tensions of solid and liquid and the interfacial tension between them.

i.e., the roughness of the surface enhances the wettability due to the surface area magnification. Lotus and some other plant leaves repel the water quite well by means of this way. In our work, fractal structure is adopted as an extremely rough surface to achieve the super water- and even oil-repellent surfaces.

There is one more theory to describe the super liquid-repellent surfaces. In the Cassie/Baxter theory,[10] the solid surface is assumed to be constructed of two components of materials 1 and 2 in mixing microscopically. Suppose the contact angles of a liquid on the surface of the pure component 1 and 2 to be θ_1 and θ_2, respectively, and the surface area fraction of component 1 and 2 in the mixed solid surface to be f_1 and f_2, respectively, the contact angle of the liquid on the microscopically mosaic surface can be expressed as

$$\cos\theta_r = f_1 \cos\theta_1 + f_2 \cos\theta_2. \tag{4}$$

When a super liquid-repellent surface is analyzed by the Cassie/Baxter equation, one component, say component 2, is assumed to be air, and the contact angle, θ_2, on the air is 180°. Then, eq (5) is obtained, since $f_1 + f_2 = 1$.

$$\cos\theta_r = f - 1 + f\cos\theta \tag{5}$$

where f_1 and θ_1 are rewritten as f and θ as the value of θ_1 in eq (4) corresponds to θ in eqs (1) and (3). The Cassie/Baxter theory is usually applied to the surfaces consisting of many pillars aligning perpendicularly to the surfaces.

Theory on the Wettability of Fractal Surface

Fractal surface is an ideal surface from the viewpoint of surface area magnification, since the surface consists of rough structure of nesting like a Russian dole. When the roughness of the surface is in fractal nature, the surface area magnification factor r in eq (3) can be written as $(L/l)^{D-2}$. Then, the contact angle θ_f of liquid droplet placed on a fractal solid surface is given by eq (6).[3,4,9]

$$\cos\theta_f = \left(\frac{L}{\ell}\right)^{D-2} \cos\theta \tag{6}$$

where L and l are the upper and the lower limit lengths of fractal (self-similar) behavior, respectively; D $(2 \leq D < 3)$ is the fractal dimension of the solid surface. Eq (6) indicates that the contact angle of liquid droplet placed on the fractal surface changes greatly when compared with the flat surfaces, since the surface area magnification factor $(L/l)^{D-2}$ can easily become large enough. Applicability of eq (6) is, however, limited. In fact, eq (6) can not give any contact angle when the absolute value of its right-hand side exceeds unity. This discrepancy originates from the assumption of full contact of liquid with the fractal solid surface. Water cannot penetrate into very small hydrophobic pores due to the capillary effect. Taking this factor into account, we have the theoretical curve of the wettability on the fractal surfaces as shown in Figure 2. One can see from the figure that a super wettable and/or a super liquid-repellent surface can be obtained by making the surface fractal.

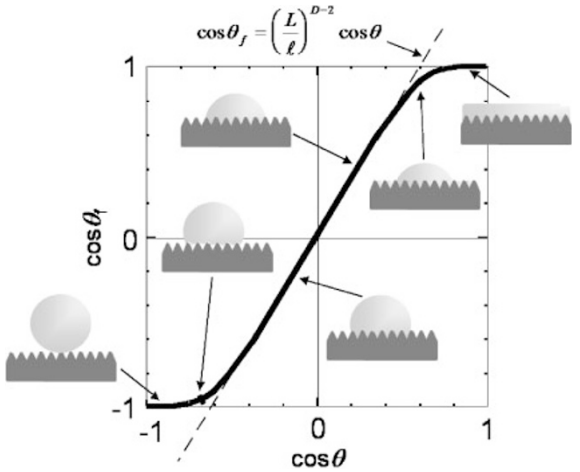

Figure 2. Schematic illustration of the relationship between $\cos\theta_f$ and $\cos\theta$ predicted theoretically.

SUPER WATER-REPELLENT FRACTAL SURFACES OF SOME WAXES

We know now theoretically that the fractal surfaces are quite powerful to make a super liquid-repellent surface. In order to realize the fractal surfaces we take some wax samples, since they form interestingly the fractal surfaces spontaneously.

Alkylketene Dimer (AKD) Wax

Alkylketene dimer (AKD; Figure 3) is a kind of wax having the melting point of about 65 °C, and forms spontaneously fractal surfaces when solidified from its melt.[3,4] Figure 4 shows the scanning electron microscopic (SEM) images of an AKD surface.[3,4] One can see from the figure that there are two kinds of structures of roughness. One has a spherical shape like a flower of hydrangea having a size of roughness of about 30 μm, and the other is a flake-like structure the size of which is about 1 μm. This stratified structure suggests that the AKD surface is fractal as actually substantiated later. A water droplet on this AKD surface is shown in Figure 5(a).[3,4] The contact angle of this water droplet is 174°. It is not easy even to put a water

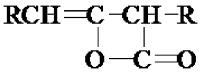

Figure 3. Molecular structure of Alkylketene Dimer (AKD). Pure AKD: R = n-C_{16}, Mixed AKD: R = n-C_{14} and n-C_{16}.

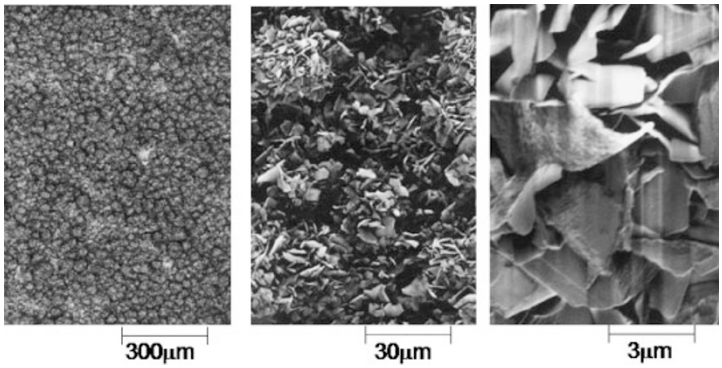

Figure 4. SEM images of an AKD surface with different magnification.

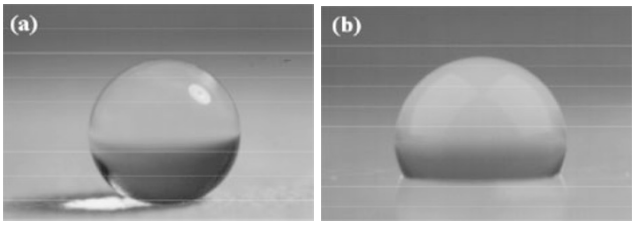

Figure 5. Water droplet (~1 mm size) on a super water-repellent AKD surface (a) and on a flat AKD surface (b).

droplet on this surface, since the droplet rolls out of the surface when tilted slightly. And then, no contact angle hysteresis on this surface was observed.

The AKD sample with a flat surface was also prepared as a reference by mechanical cutting with a knife. The flat surface is, of course, not very water-repellent, showing the contact angle of 109° (Figure 5(b)). One can understand now that the super water-repellency of the surface can be realized by the surface roughness of the AKD.

Let us confirm that the rough surface of AKD is in fractal nature. Box counting method is widely used to estimate a fractal dimension. Self-similarity and the fractal dimension D can be evaluated by the following relationship.[1]

$$N(r) \propto r^{-D} \tag{7}$$

where r is the size of boxes, N(r) is the number of boxes to cover the target object, and D is the fractal dimension of the object. The fractal dimension D can be obtained from the slope of the log N(r) *vs.* log r plot.

The fractal dimension of cross section D_{cross} ($1 \leq D_{\mathrm{cross}} < 2$) has been measured by the box counting method. The fractal dimension D of the surface has been evaluated as $D \cong D_{\mathrm{cross}} + 1$.[11] Figure 6 demonstrates the SEM images of the cross section of an AKD surface shown in Figure 4. Trace curves of the solid surface were drawn from the cross-sectional SEM images, and shown in Figure 7. Figure 8 shows the log N(r) against log r plot for the AKD surface made from the trace curves of Figure 7. The slope of the straight line gives us the fractal dimension of the surface structure. One can see clearly that the straight line has two break points at $r = 0.2\,\mu\mathrm{m}$ (l) and $r = 34\,\mu\mathrm{m}$ (L), and two different slopes. One slope is

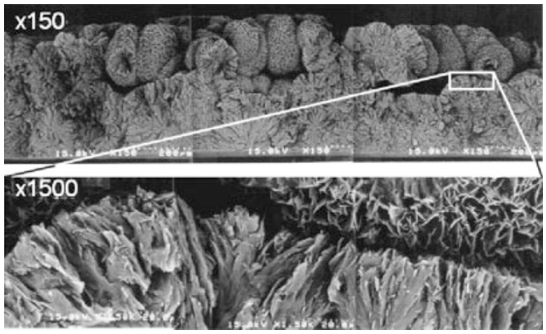

Figure 6. SEM images of a cross section of AKD surface with different magnification.

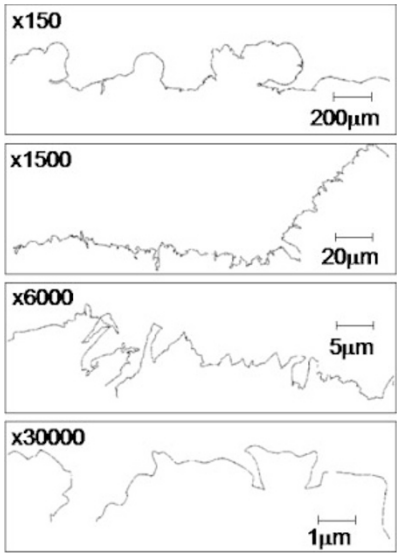

Figure 7. Trace curves of the cross section of a super water-repellent AKD surface. Tracing was made for the SEM images shown in Figure 6.

-1.29 between the two critical sizes, and the other is -1 in the range of their outside. So, the cross section of the surface is fractal with the dimension of $D_{\mathrm{cross}} = 1.29$ and the fractal structure (self similarity) is found to hold between $L = 34\,\mu\mathrm{m}$ and $l = 0.2\,\mu\mathrm{m}$. The fractal dimension of the surface was, then, evaluated to be 2.29. Two critical sizes of $L = 34\,\mu\mathrm{m}$ and

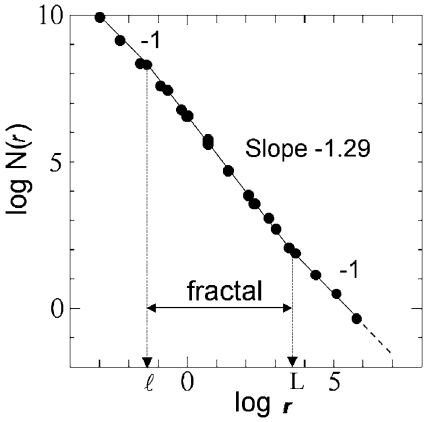

Figure 8. The plots of log N(r) *vs.* log r for the cross-sectional trace curve of an AKD surface.

$l = 0.2\,\mu m$ interestingly correspond quite well to the sizes of the flower-like structure and the thickness of the flake-like crystal of the AKD. One can easily imagine that the surface is flat (2-dimensional) when observed with the larger scale than the spherical flower-like structure. The surface is also flat for the water droplet of smaller size than the thickness of the flake-like crystal. Now, the AKD surface is substantiated to be fractal.

Triglyceride Waxes

We have another wax samples showing the super water-repellent fractal surfaces. They are triglycerides. Spontaneous formation of super water-repellent triglyceride surfaces at different temperatures was monitored by the time-dependent contact angles of water, as shown in Figures 9 for tristearin (SSS) as an example.[12] The result in this figure shows the progressive formation of the super water-repellent surface of SSS. The freshly solidified triglyceride surfaces from the melt are translucent and the initial contact angles of water on them are close to 110°. The surfaces then become rough and clouded after incubated for a certain time at a specified temperature, which is well known as "blooming phenomenon"[13] in the chocolate industries. The contact angle on the rough and clouded surface increases with time at each temperature, and becomes greater than 150° at the final stage of this process.

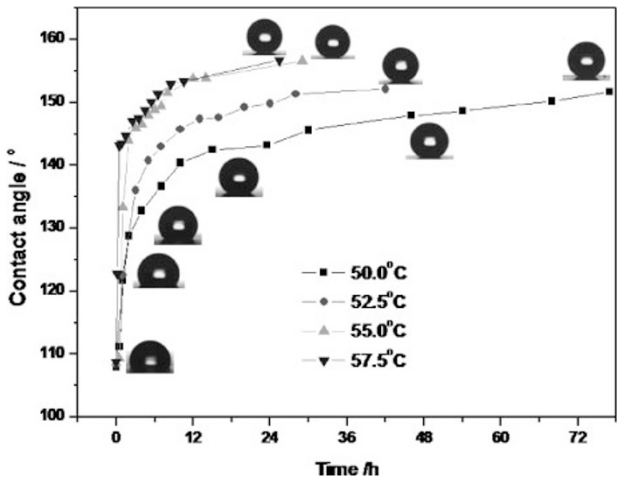

Figure 9. Time-dependent contact angles and some photographs of water droplets on the tristearin (SSS) surfaces cured at different temperatures.

SEM images of different magnifications for the super water-repellent triglyceride surfaces are shown in Figure 10.[12] The beautiful rough structures are clearly seen, and the roughness enhances the water-repellency. The SEM images with several magnifications of the cross sections of the rough triglyceride surfaces were used to determine the fractal dimension. The fractal dimensions of the trimyristin (MMM), tripalmitin (PPP) and SSS surfaces were calculated to be 2.21, 2.24 and 2.23, respectively.[12] The super water-repellency of triglyceride waxes are now understood to be also originated from the fractal structures of their surfaces.

FORMATION MECHANISM OF FRACTAL STRUCTURES ON WAX SURFACES

As mentioned before, AKD and triglycerides form fractal structures spontaneously on their surfaces made by the solidification from their melts, and give super water-repellency.[3,4,12] But the reason why the fractal surfaces form spontaneously is not clear yet. A preliminary research suggested that the mechanism of spontaneous formation of fractal structures on AKD surface originated from a phase transformation from a meta-stable to a stable crystalline form.[14] Then, we have studied the mechanism of spontaneous formation of fractal structures on wax surfaces to confirm the above hypothesis.

Triglyceride Waxes

Triglycerides are first chosen as the wax samples, since the phase transition from a meta-stable to a stable crystalline form ("blooming phenomenon")[13] is well known during their crystallization process from the melts. The complex polymorphic phenomenon of triglycerides has been extensively investigated.[13,15–20] Triglycerides have three main polymorphic states, α, β' and β, which have different melting points. The α and β' forms are in meta-stable state and the β form is in the thermodynamically stable one at room temperature and atmospheric pressure. The β' form is hardly observed. Figure 11 shows the Differential Scanning Calorimetric (DSC) curves for three triglyceride samples having three different retention histories; the freshly solidified triglycerides (11a, 11d and 11g), the super water-repellent surfaces (11b, 11e and 11h), and the stable triglycerides (11c, 11f and 11i) which have been stored for long time (more than one year).

It is clear from Figure 11 that there exist three peaks for the fresh samples, particularly for PPP and SSS. Two endothermic peaks correspond to the melting of the α (lower temperature) and β (higher temperature) forms, respectively. The exothermic peak corresponds to the crystallization from the α form in meta-stable state to the stable β form. When the α form transforms directly to the β form without noticeable melting, the endothermic peak does not appear. This may be the case in

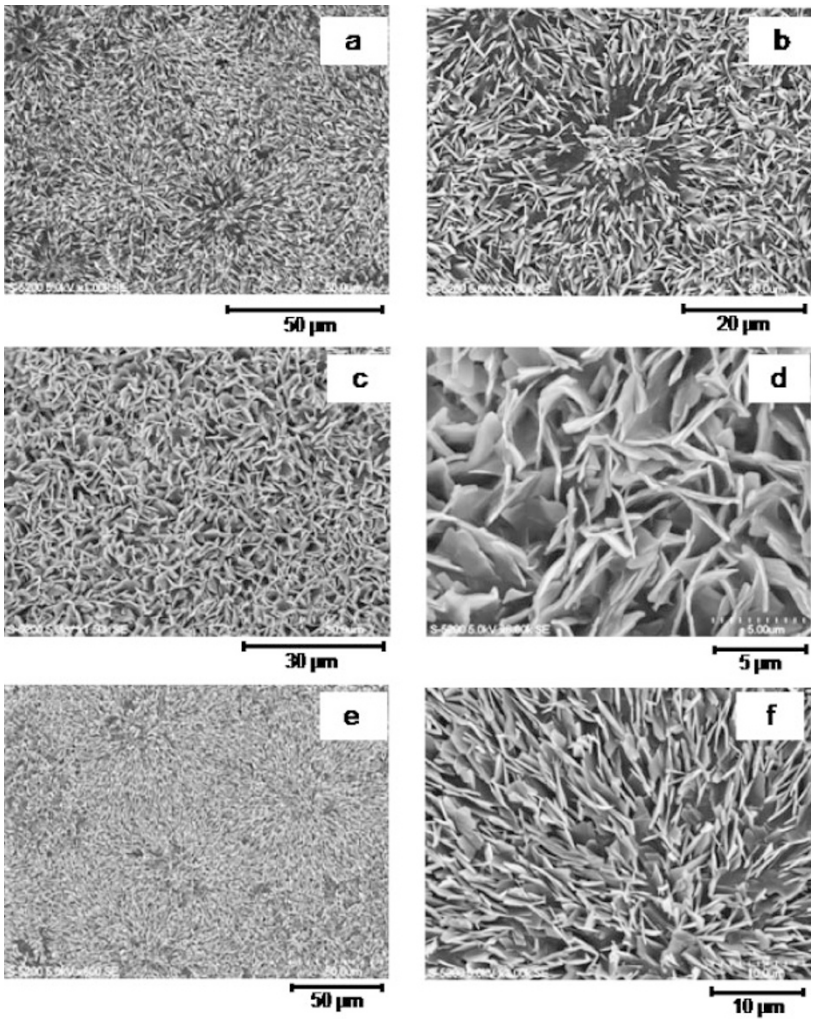

Figure 10. SEM images of the super water-repellent triglyceride surfaces. MMM (trimyristin); a and b, PPP (tripalmitin); c and d, and SSS (tristearin); e and f.

the transition of MMM (Figure 11a). In the DSC curves for the samples of the super water-repellent surfaces and the aged triglycerides, the melting and crystallization peaks of the α form disappear. The meta-stable α form might undergo a solid-melt-solid or a solid-solid transformation into the stable β form, resulting in the increase of the roughness of the surfaces. These results indicate that the growth of the rough and water-repellent triglyceride surfaces takes place during the phase transformation from the meta-stable state to the stable one.

Furthermore, X-ray diffraction (XRD) patterns were recorded for the freshly solidified PPP and SSS samples at some time and temperature intervals, using temperature-controlled X-ray diffractometry. The results are presented in Figure 12. The initial record of XRD pattern was performed at 28 °C. The sample was then heated to the next temperature at the heating rate of 2 °C/min and was kept at that temperature for 10 minutes before measurement. At each temperature, two separate records were carried out with the time interval of 2 h.

In the wide angle region shown in Figure 12, the samples of the freshly solidified triglyceride crystal have a single strong refelection at $2\theta = 21.5^\circ$ ($d = 0.415$ nm) indicating the α state.[16] The stable β state is typically characterized by the very strong refelection at $2\theta = 19.3^\circ$ ($d = 0.460$ nm). With the increase of the temperature, triglycerides undergo a thermally activated transformation from the meta-stable state to the stable crystalline one. The peaks of β state become sharper and sharper, and their intensities become stronger and stronger. It shows the growth of the stable crystal and the increase of the dgree of crystallization.

From the results of DSC and XRD measurements shown in Figures 11 and 12, one can understand clearly that the fresh triglyceride crystals made by the rapid solidification from the melts are in the meta-stable α state. Under heat-treatment of the samples at a specified temperature, the meta-stable phase spontaneously transforms into the thermodynamically favorable crystalline form.

The formation mechanism of fractal structures on AKD surfaces was also studied by the same experimental manner, and the same mechanism, *i.e.*, the phase transition from meta-stable to stable crystalline form was established.[21]

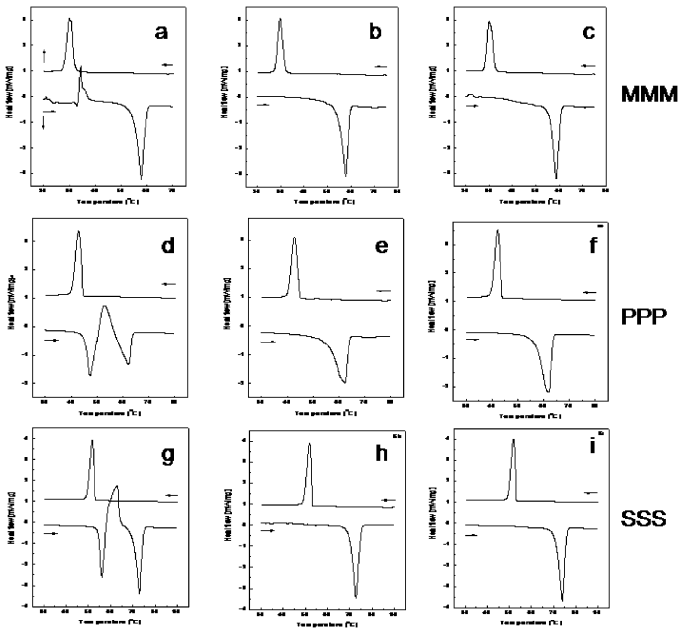

Figure 11. DSC thermograms of triglyceride waxes; MMM (trimyristin), PPP (tripalmitin) and SSS (tristearin). Freshly solidified (a, d, g), super water-repellent (b, e, h) and stable samples (c, f, i). ↑: exothermic, ↓: endothermic, →: heating, ←: cooling Heating rate: 3 °C/min.

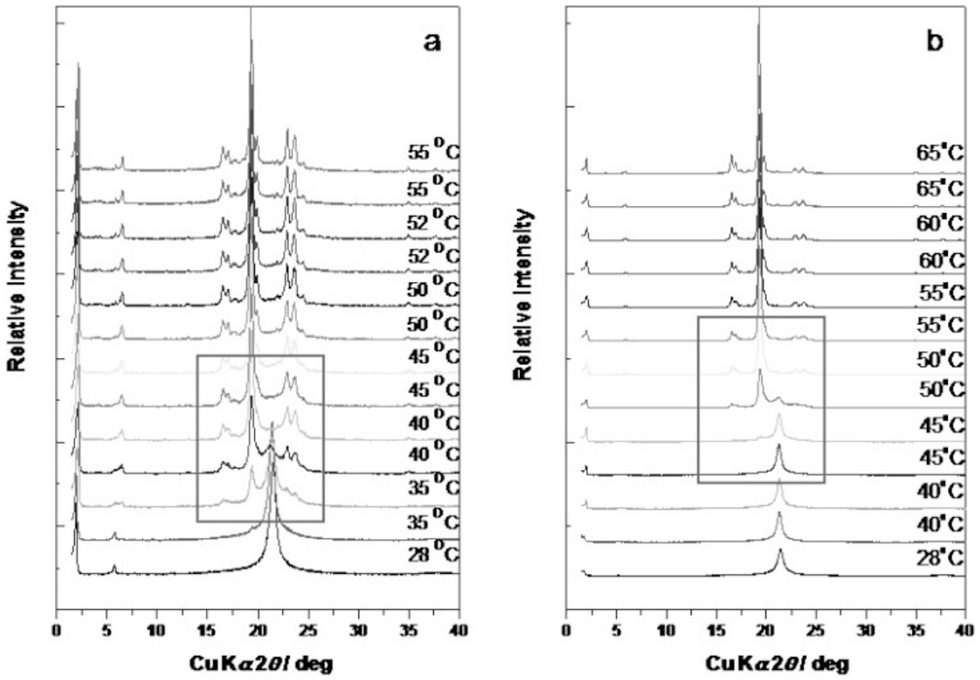

Figure 12. XRD patterns of PPP (a) and SSS (b) at different temperatures. The initial record was performed at 28 °C. The sample was then heated to the next temperature at the heating rate of 2 °C/min and was held for 10 min. Two records were carried out with the time interval of 2 h at each temperature.

Generalization of the Mechanism by Extension of the Investigation to Other Waxes

We know now the reason why the fractal structures form spontaneously on the surfaces of AKD and triglyceride waxes. But we have just two examples at present to exhibit such mechanism. In order to generalize the above mechanism we have to extend the investigation to other waxes as many as possible. We have examined 15 wax samples for generalization of the formation mechanism of the fractal structures.[22] Thus, this section deals with the surface structures, super water-repellency and the phase transition behaviors of various wax samples in order to obtain the general rule for the spontaneous formation of fractal structures on wax surfaces. Furthermore tempering operation is applied to some wax samples which give the super water-repellent fractal surfaces. Tempering is a technique to make the triglycerides transform directly to the

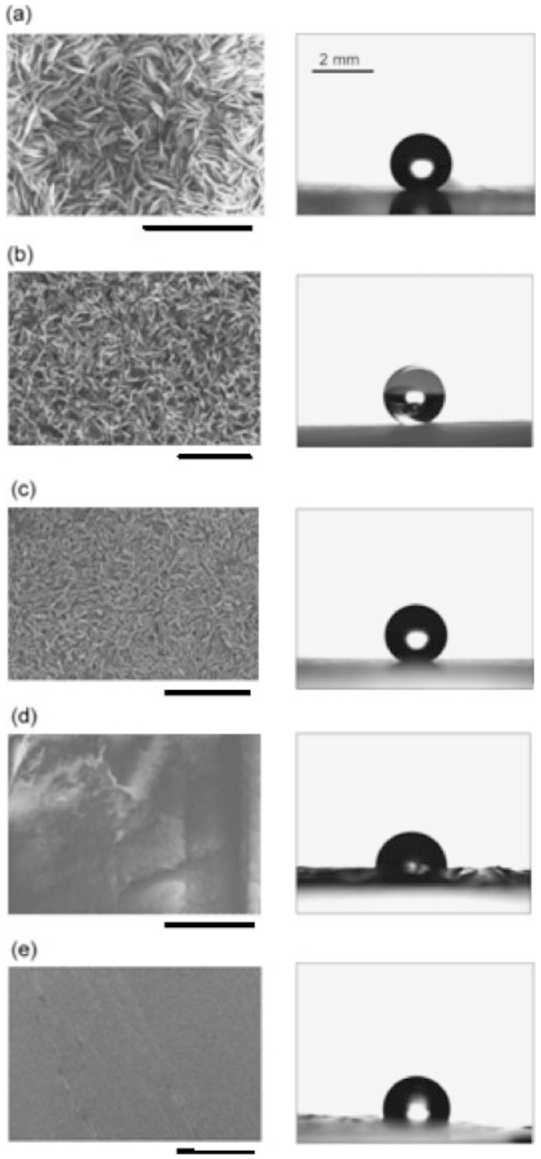

Figure 13. SEM images (left) of mixed AKD (a), distearin (b), tristearin (c), lauric acid (d) and dotriacontane (e), and photos of a water droplet on their surfaces (right). The bars in the SEM images represent 30 μm.

stable β-crystal from their melts, and has been developed in the chocolate industries to avoid the "blooming phenomenon."

Figure 13 shows some examples of the surface structure (SEM image) of wax samples annealed for several hours just below their melting temperature, and the photograph of a water droplet placed on them.[22] As can be seen clearly, three wax samples (mixed AKD; mixed alkyl chain length of C_{14} and C_{16}, distearin and SSS) give rough surfaces and exhibit super water-repellency (contact angle $> 150°$). The other two samples (lauric acid and dotriacontane) form smooth surface and show normal wettability. The contact angles and the surface structures for all samples tested are summarized in Table I.[22]

In order to understand the common property in phase behaviors of three wax samples showing the super water-repellency, DSC thermograms were observed for all the wax samples. As mentioned previously, AKD and triglyceride waxes show the melting of meta-stable crystalline form and the phase transition to the stable one in their DSC curves. However, in the lauric acid sample, for example, two thermograms in the first and the second run are the same.[22] This result means that lauric acid has no meta-stable form of crystal when solidified from its melt. Existence or nonexistence of meta-stable crystalline phase of all the wax samples tested is also summarized in Table I.[22] One can recognize from the table that the super water-repellent fractal surfaces form spontaneously during the phase transition from a meta-stable to a stable crystalline form without any exceptions at least for the wax samples tested.[22]

Table I. Contact angle, surface structure and the existence of meta-stable crystalline form of wax samples

Wax	Contact angle	Surface structure	Meta-stable phase
Mixed AKD	151° ± 2°	fractal structure	Yes
Lauric acid	86° ± 5°	flat and smooth	No
Stearic acid	89° ± 5°	flat and smooth	No
Behenic acid	113° ± 6°	flat and smooth	No
Enicic acid	83° ± 2°	flat and smooth	No
Cetyl alcohol	61° ± 4°	flat and smooth	No
Steaiyl alcohol	93° ± 2°	flat and smooth	No
Heneicosane	109° ± 3°	flat and smooth	No
Dotriacontane	108° ± 3°	flat and smooth	No
Hexatricontane	105° ± 1°	flat and smooth	No
Palmityl palmitate	107° ± 1°	flat and smooth	No
Steaiyl stearate	106° ± 2°	flat and smooth	No
Monostearin	81° ± 1°	flat and smooth	No
Distearin	153° ± 2°	fractal structure	Yes
Tristearin	154° ± 2°	fractal structure	Yes

Tempering operation is a method to make the triglycerides transform directly to the stable β form from their melts without passing through the meta-stable α form. In this method the crystallization of triglycerides from their melts is carried out at the temperature between the melting points of the meta-stable and the stable form of crystals. Figure 14 shows the SEM images of the surfaces of mixed AKD, pure AKD (pure alkyl chain length of C_{16}) and PPP after tempering operation. One can see the obvious change of the surface roughness of the pure and mixed AKD samples, comparing the SEM image in Figures 3 and 13(a), respectively. The fractal rough structure disappears after the tempering operation. The photographs of the water droplets on the tempered AKD and PPP surface are shown in Figure 15. The contact angles are quite normal, and the AKD and PPP waxes do not show the super water-repellency.[22]

The DSC thermograms for mixed AKD, pure AKD and PPP are shown in Figure 16. They do not have endothermic peak at lower temperature, but show only the melting peak of the stable form of crystal. These experimental results strongly indicate that the tempering operation works quite well and the 3 wax samples transform directly to the stable crystalline form from their melt.[22]

As reported previously, AKD and triglycerides form the super water-repellent fractal surfaces during the phase transition from the meta-stable crystalline form to the stable

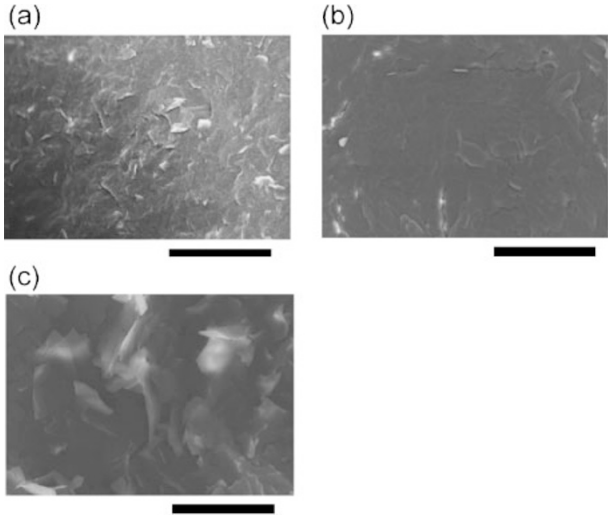

Figure 14. SEM images of surfaces of mixed AKD (a), pure AKD (b) and PPP (c) after tempering operation. The bars represent 30 μm.

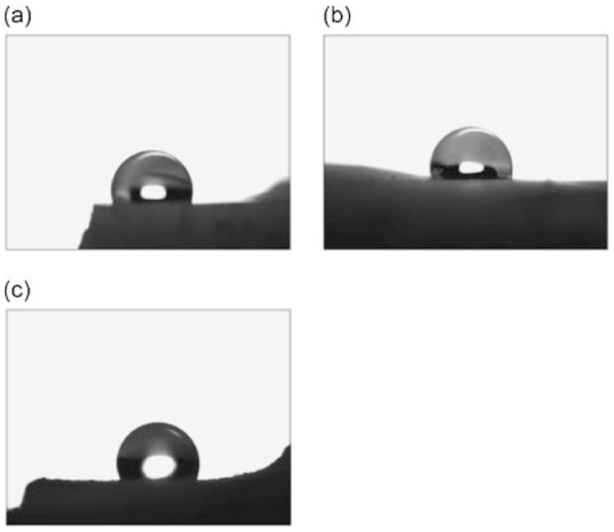

Figure 15. Photos of water droplets on mixed AKD (a), pure AKD (b) and PPP (c) after tempering operation. Contact angles are 110° ± 0°, 109° ± 2° and 109° ± 4° for (a), (b) and (c), respectively.

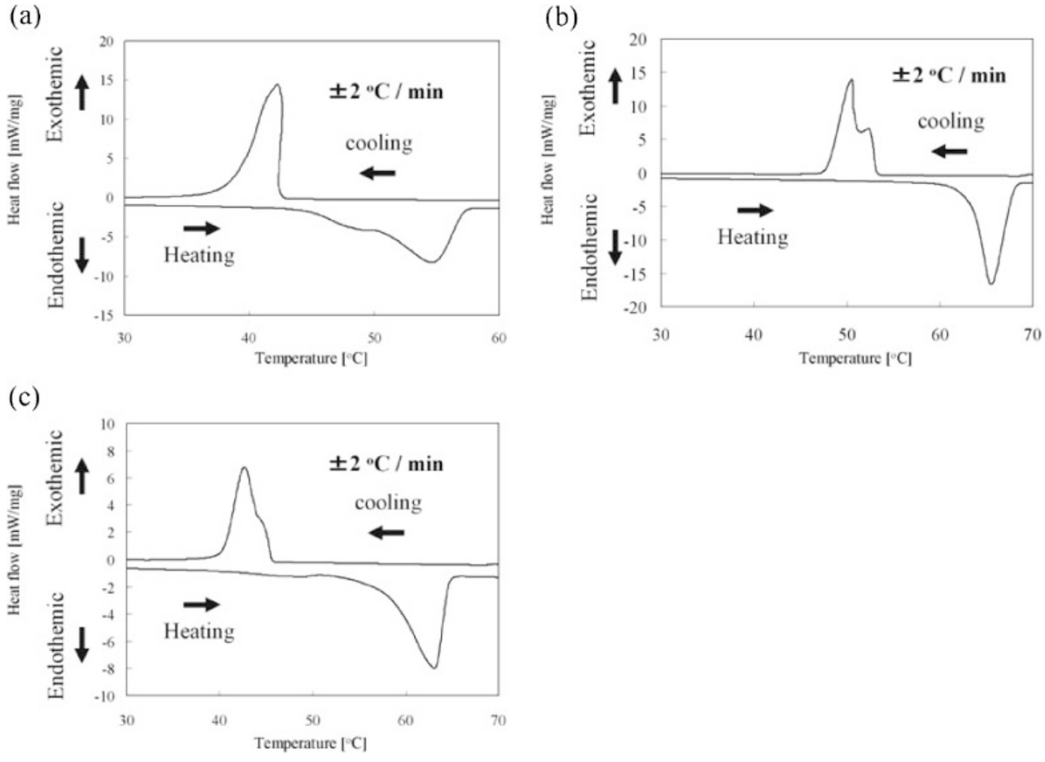

Figure 16. DSC curves in first run of mixed AKD (a), pure AKD (b) and PPP (c) after tempering operation.

form.[12,21] This empirical rule has been extended to various waxes without any exceptions in this section.[22] The wax samples of AKD, diglyceride and triglyceride have meta-stable form of crystal and give super water-repellent fractal surfaces. Any other waxes have no meta-stable crystalline phase and do not form the fractal surfaces. The empirical rule mentioned above may be the general one at least for the waxes tested here.[22] Figure 17 shows the schematic Gibbs free energy curves to explain the formation mechanism of fractal structures on wax surfaces, although we still do not know why the structure is fractal.

SUPER OIL-REPELLENT ALUMINUM OXIDE SURFACES

We can apply the same theory, *i.e.*, enhancement of wettability by fractal structure of surfaces, also to the novel super oil-repellent surfaces. The highest barrier to obtain the

super oil-repellent surface is to make a flat surface which has a contact angle greater than 90° for oils. Let us estimate the surface tension of the solid to achieve the above condition. According to the Young's eq (1), the surface tension of solid surface (γ_S) must be equal to the interfacial tension between solid and liquid (γ_{SL}) when the contact angle is 90°. The interfacial tension, γ_{SL}, can be approximately expressed by the following eq (8), when the interaction force between the two materials is same kind.[23]

$$\gamma_{SL} = \gamma_S + \gamma_L - 2\sqrt{\gamma_S \gamma_L} \quad (8)$$

Combining Eqs (1) and (8), we obtain $\gamma_S = \gamma_L/4$ for the condition of $\theta = 90°$. Typical surface tensions of oils are 20–30 mN/m, and the value of γ_S must be the order of several mN/m. So small surface tension of solid can be provided only by the trifluoromethyl group.[24] Accordingly, our strategy to make the super oil-repellent surfaces is to obtain a fractal surface of enough roughness and then cover the rough surface with trifluoromethyl groups by treating it with some fluorinated compound.[5,6]

The anodically oxidized aluminum surface was employed as the fractal surface for this purpose and was hydrophobized by treating it with the fluorinated monoalkylphosphates (n-$CF_3(CF_2)_mCH_2CH_2OP(=O)(OH)_2$, m = 7 or 9; abbreviated as F_{m+1}-MAP). Figure 18 shows the SEM images of anodically oxidized aluminum surfaces with different magnifications. The fractal analysis was performed for these surfaces. The box counting method was applied again to the tracing image of the cross section of the above surfaces and the fractal dimension of the surfaces was estimated to be 2.16–2.19. The upper (L) and the lower limit size (l) in eq (6) could not be obtained in this case, and unfortunately the roughness factor $(L/l)^{D-2}$ was not estimated.

An anodically oxidized aluminum plate was washed with pure water and then immersed in 2.0 wt % ethanol solution of F_8-MAP or F_{10}-MAP for 1 week at room temperature. The thickness of the F_{m+1}-MAP film on the treated aluminum surface was not clear, but the monolayer adsorption could be expected. An oil droplet of rape-seed put on the treated anode-oxidized aluminum surface is demonstrated in Figure 19.[5,6] One can see a beautiful spherical shape of the oil droplet having a very high contact angle of 150°. The oil droplet having so high contact angle rolls around without attaching on the surface when tilted slightly indicating small contact angle hysteresis. This super oil-repellent surface is, unfortunately, not durable probably because of the weak adsorption of the treating agent.

The contact angles of various oils and their surface tension values are summarized in Table II.[6] Oil repellent surfaces treated with F_{10}-MAP having a contact angle greater than

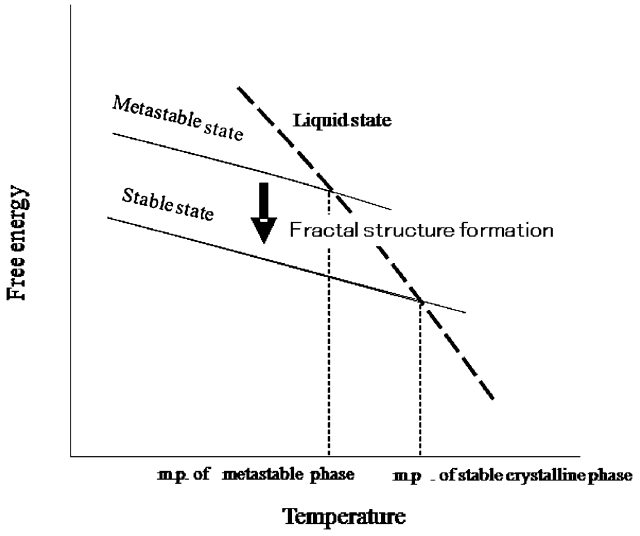

Figure 17. Free energy relationship among the meta-stable, stable crystals and the liquid state to explain the spontaneous formation of fractal structures on wax surfaces.

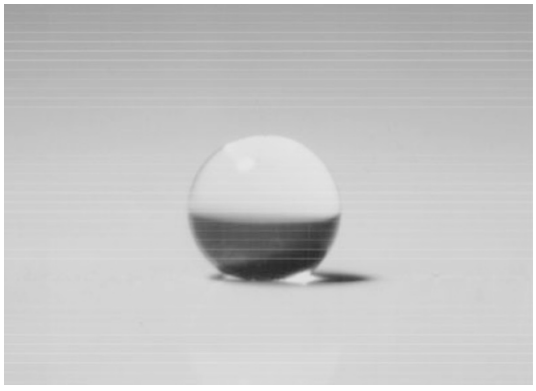

Figure 19. A droplet of rape-seed oil on a super oil-repellent surface.

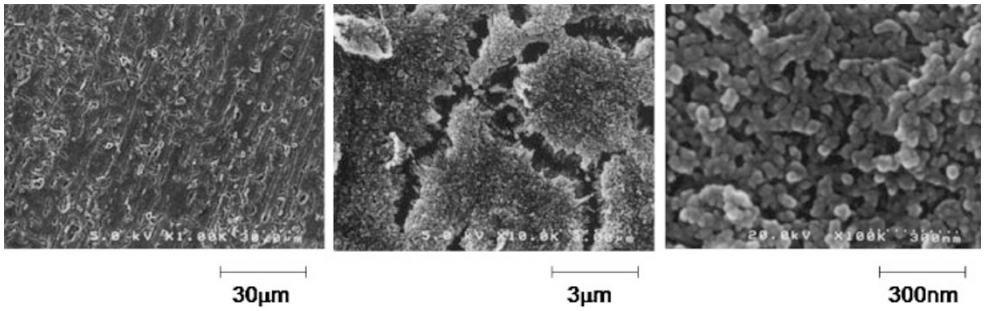

Figure 18. SEM images of anodically oxidized aluminum surfaces with different magnifications. These surfaces are also fractal.

Table II. Contact angles of various oils on the super oil-repellent and flat aluminum surfaces

		Contact Angle/deg.						
		un-treated	F_8-MAP		F_{10}-MAP		Si-coupling	
Oil	Surface tension mN/m	θ	θ	θ_f	θ	θ_f	θ	θ_f
Hexane	18.4	6.5	33.3		28.8	23.5	27.0	17.0
Octane	21.6	5.0	45.8	47.5	46.6	105.3	43.9	42.5
Decane	23.8	6.2	62.3	90.0	57.0	127.6	51.8	90.0
Dodecane	25.4	6.3	75.5	90.0	69.8	127.0	62.6	97.9
Hexadecane	27.5	3.8	86.4	115.0	75.5	135.5	71.5	105.6
Amyl Alcohol	25.8	6.1	61.6	113.4	70.5	122.8	46.8	29.9
Octanol	27.5	3.6	72.8	129.6	72.8	124.9	52.6	35.6
Dodecanol	29.4	16.4	90.0	130.5	80.3	130.6	57.6	95.0
Cyclohexane	33.4	19.3	84.4	139.0	90.0	127.6	58.5	67.2
Diethylene Glycol	45.2	60.7	102.4	152.0	99.2	135.0	76.2	146.0
Glycerol	63.4	75.6	129.5	161.2	120.0	134.9	96.6	154.2
Methyl Myristate	29.4	8.5	91.6	131.6	76.6	132.3	48.5	60.2
Diethyl Glutarate	32.3	16.4	88.8	132.4	74.8	134.0	52.0	52.1
Diethyl Adipate	36.0	29.6	96.5		72.3	139.3	53.2	67.8
Dimethyl Malonate	37.4	47.5	101.2	140.5	72.0	152.8	60.0	78.6
Monoacetin	41.8	45.9	110.0	150.6	104.2	153.3	67.2	131.0
p-Xylene	30.7	10.5	75.0	126.2	67.5	127.0	50.0	51.4
Chlorobenzene	36.0	20.2	81.8	121.5	63.5	128.1	52.5	62.0
Ethyl benzoate	37.2	25.6	90.0	137.1	79.5	140.5	53.2	46.8
Benzyl Chloride	40.0	28.4	90.0	136.6	83.5	146.5	64.7	92.5
Water	72.3	92.6	114.4	163.0	119.0	166.0	108.0	161.0

The contact angles θ_f on the untreated fractal surface were ~0° for every liquid

120° have been achieved for oils with a surface tension of approximately 24 mN/m of decane. The critical surface tension of the treated flat aluminum surface can be estimated to be 14–15 mN/m by the Zisman plot using the data in Table II.[6] This value is still far from the surface tension of trifluoromethyl group (~ 6 mN/m) implying that the treating agent molecules are not packed densely enough or lie on the surfaces at least in part. The very high advancing contact angle of 160° for octane has been reported very recently utilizing very sophisticated hoodoo-type micro-structures on the surfaces.[25] This technique is an application of the pinning effect of wetting.[26]

DURABLE SUPER WATER- AND HIGHLY OIL-REPELLENT SURFACES

As mentioned previously, the AKD surface shows the contact angle for water of 174°. The AKD surface, however, has a drawback of poor durability from the standpoint of practical applications. The AKD surface is environmentally weak mainly because of its soluble nature in organic solvents, low melting point of about 65 °C and relatively poor chemical stability. Therefore, creation of environmentally stable super water-repellent surfaces is crucially of significance in practical applications.

Conductive polymers have attracted great attention because of its unique electrical properties and easy synthesis of film-shaped products coupled with good thermal and solvent stability.[27–29] And, the synthetic methods have been well established.[30,31] Conventionally, the conductive polymers are electrochemically synthesized as films with various surface features depending on the reaction conditions.[31] Thus in principle, the conductive polymer films with fractal structure or rough morphology are easily synthesized by simple optimization of the reaction conditions. Kossmehl *et al.* previously reported poly(2,2′-bithienyl-5,5′-diyl) (PBT) layers which were synthesized by an electrochemical method, and showed super water-repellency and good thermal stability.[32,33] Then, we tried to synthesize the super water-repellent poly-(alkylprrole) films with excellent environmental stability to both temperature and organic solvents or oils.[34,35]

Electrochemical Synthesis and Characterization of Poly-(alkylpyrrole) Films

The electrochemical synthesis was performed in a two-electrode cell containing acetonitrile solution of alkylpyrrole and sodium *p*-toluenesulfonate as an electrolyte and/or a dopant by using a constant current generator.[34,35] In this work 1-*n*-octadecylpyrrole was used as an alkylpyrrole. The electrochemical synthesis was carried out under certain typical conditions as follows: working electrode, indium-tin-oxide (ITO) glass; 1-*n*-octadecylpyrrole, 5 mM; sodium *p*-toluenesulfonate, 0.5 mM; applied voltage, 22.5 V; reaction time, 60 min.

Figure 20 shows the poly(alkylpyrrole) film electrochemically synthesized using 1-*n*-octadecylpyrrole and sodium *p*-toluenesulfonate as a monomer and an electrolyte, respectively.[34] Quite interestingly, "needle"-like shaped poly(alkylpyrrole) grows perpendicularly to the surface of the ITO electrode. Thousands of the "needle"-like shaped poly(alkylpyrrole) in sizes of *ca.* 5 μm in diameter and *ca.* 40 μm in length are orderly arrayed in the surface of the ITO electrode.

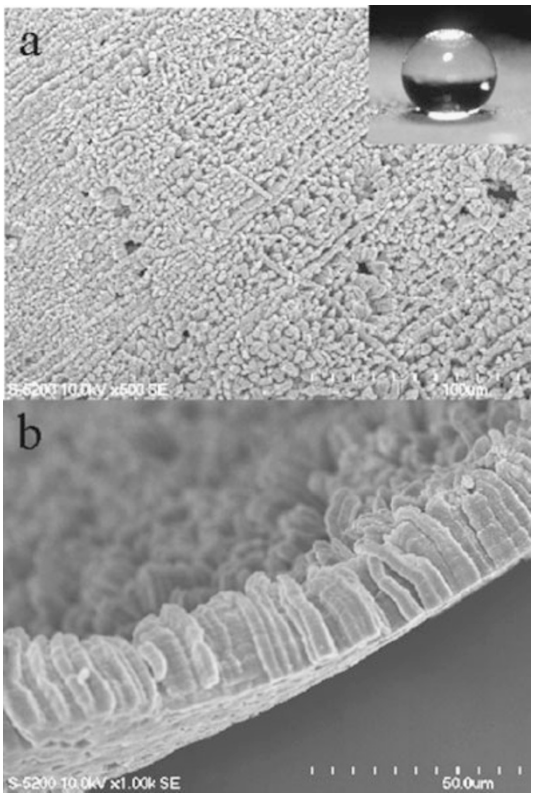

Figure 20. Scanning electron microscopic (SEM) image of surface (a) and cross-section (b) of the produced poly(alkylpyrrole) film. Inset is a digital camera image of a water droplet (~1.5 mm diameter) on the film.

Super Water-Repellency and Environmental Stability of Poly(alkylpyrrole) Films

The features of the array on the poly(alkylpyrrole) films should show super water-repellency in principle. Furthermore, the array should show high stability to heating and organic solvents because the conductive polymers usually consist of long range conjugated aromatic rings which are thermally stable and poorly soluble in usual organic solvents.[31]

Actually the surface of the poly(alkylpyrrole) film showed super water-repellency with a contact angle larger than 150°, as shown in the inset of Figure 20.[35] The surface of the poly(alkylpyrrole) film was analyzed on the cross section of the film by a box counting method, and found to be fractal with a dimension of ~2.2.[34,35]

Thermal stability was evaluated by treating the films at various temperatures for 2 h. After the thermal treatments, the contact angles were measured at room temperature. Figure 21 shows the effect of the treating temperature on the contact angle for water on the film.[34,35] The contact angle of the film was nearly constant even when the treating temperature increases. The inset in Figure 21 shows the effect of the treating time at 80 °C on the film. The contact angle of the film was also nearly constant even when the treating time increases. The poly(alkylpyrrole) is one of the conductive polymers which usually consists of aromatic rings and conjugated π-bonds on the main polymer chains. Therefore, the polymer has

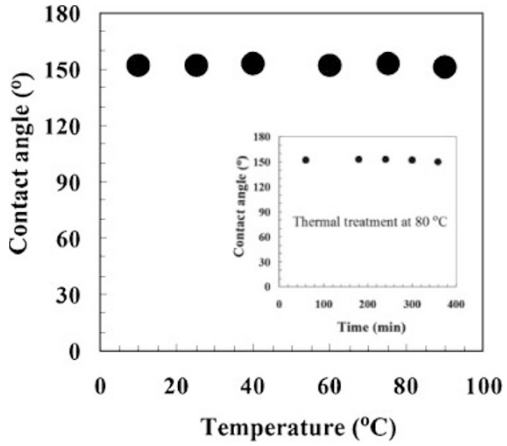

Figure 21. Thermal stability of the super water-repellent poly(alkylpyrrole) film. The contact angle does not change after treatment at high temperatures.

enough thermal stability of chemical composition in the experimental range of the temperature and the treating time.

Similarly the influences of organic solvent- and oil-treatment on the wettability are systematically investigated in order to evaluate the durability of the films toward the organic solvents and oils in terms of contact angle for water. The contact angle of the film did not change even after the treatments with various solvents and oils. We have now succeeded in making the durable super water-repellent films at least for the thermal and solvent-treatment stability.[34,35]

Highly Oil-Repellent Poly(alkylpyrrole) Films

We have tried to convert the durable super water-repellent poly(alkylpyrrole) films to the oil-repellent ones.[36] Coating of fluorinated alkylsilane coupling agent on "needle"-like shaped surface of poly(alkylpyrrole) films was carried out. The coated film showed the contact angles larger than 150° and 130° for water and salad oil, respectively.[36] The SEM images showed that the geometrical structure of the film surface did not change during the coating process. The film also showed excellent stability for heating and organic solvent treatments in terms of the contact angles for both water and salad oil. The X-ray photospectroscopic (XPS) and infrared spectroscopic (IR) data revealed that thin layer of condensed heptadecafluorodecyltri-*iso*-propoxylsilane (HDFDTPS) covered homogeneously on the "needle"-like surface of the poly(alkylpyrrole) film even though without any thermal treatment.[36]

CREATION OF FRACTAL BODY BY A NOVEL TEMPLATE METHOD

We have discussed so far the fractal structure formation on some solid surfaces and their super water- and/or oil-repellent properties. In this section, we deal with the fractal body instead of surfaces. A fractal body having a fractal dimension between 2 and 3 has zero volume and infinite surface area in pure mathematical sense. It is, of course, impossible to have a body of zero volume and infinite surface area in our real physical

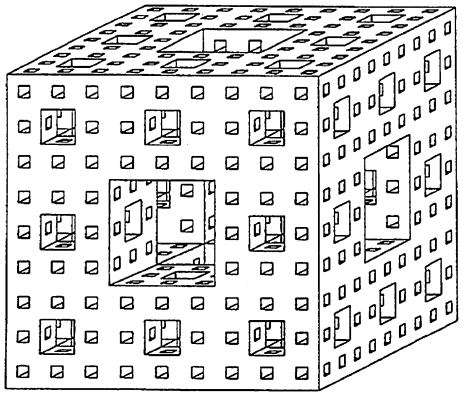

Figure 22. Menger's sponge; a typical mathematical model of fractal body. Fractal dimension = $\log 20/\log 3 \approx 2.727$. Fractal dimension of cross section = $\log 8/\log 3 \approx 1.892$.

world, but one can expect to obtain a body having very small volume and very large surface area if we can make a fractal body like Menger's sponge (Figure 22). In this section, a method to prepare a Menger's sponge-like fractal body is given, since such a fractal body has been reported to show an interesting property.[37]

Preparation Strategy of Menger's Sponge-like Fractal Body

We designed the strategy to make fractal bodies as follows.[38] The essence of this method was to utilize "fractal particles" of AKD (Figure 23(a) and 23(b)), *i.e.*, AKD particles with "fractal surface structure," as templates corresponding to pores in Menger's sponge. If we would fill remained space between the densely packed fractal particles with a suitable monomer solution (Figure 23(c) and 23(d)), solidified it (Figure 23(d)) and removed the particles by any method (Figure 23(e)), then a fractal body would be created (Figure 23(f)). The advantage of this strategy is to create a continuous fractal structure between two characteristic scales (cutoffs) of the fractal particle, *i.e.*, thickness of the flake-like crystal and the particle size as mentioned in the previous section of AKD wax. In order to control the fractal dimension, D, we compress the packed template particles (Figure 23(c)), and then we can change the size of remained space between the particles.

Preparation of Template AKD Particles and a Fractal Body by Sol-Gel Process

AKD was dissolved into *n*-hexane at *ca.* 5 wt %. AKD particles were prepared by spraying of the solution using nitrogen gas and then leaving them stand at room temperature for at least several days to form fractal surface structure of the particles spontaneously. The spontaneous formation of the fractal surfaces was observed by SEM. Figure 24(a) shows typical SEM images of different AKD particles with time course.[38] At $t = 0$ h, the surface was smooth, but, at $t = 24$ h flake-like structure appeared and began to grow like a flower. At $t = 48$ h, a flower-like surface structure was formed, and fully bloomed after 4 weeks.

Fractal AKD particles were packed into a vessel. The packed AKD particles were compressed under the compaction ratio $r_c = 1$, 2 and 3, where $r_c = 1$ means the natural packing of template particles, whereas $r_c = 2$ and 3 mean that the stacked templates were compressed to the volume ratio of $1/r_c$. In order to mold the remained space between template particles, we adopted a sol-gel reaction of TMOS.[39] The TMOS solution was added gently into the compressed templates, where the solution was the mixture of TMOS, pure water and methanol at 1:4:5 in molar ratio at pH = 6.86. They were stood at room temperature for 3 d for the sol-gel reaction. Then, they were calcined at 500 °C ($r_c = 1$) and 650 °C ($r_c = 2$ and 3) for 2 h in ambient air.

Characterization of the Fractal Bodies

After the calcinations of sol-gel product, the densities of porous silica at $r_c = 1$, 2 and 3 were measured to be 0.35, 0.20 and 0.1 g cm^{-3}, respectively. The silica which was prepared by

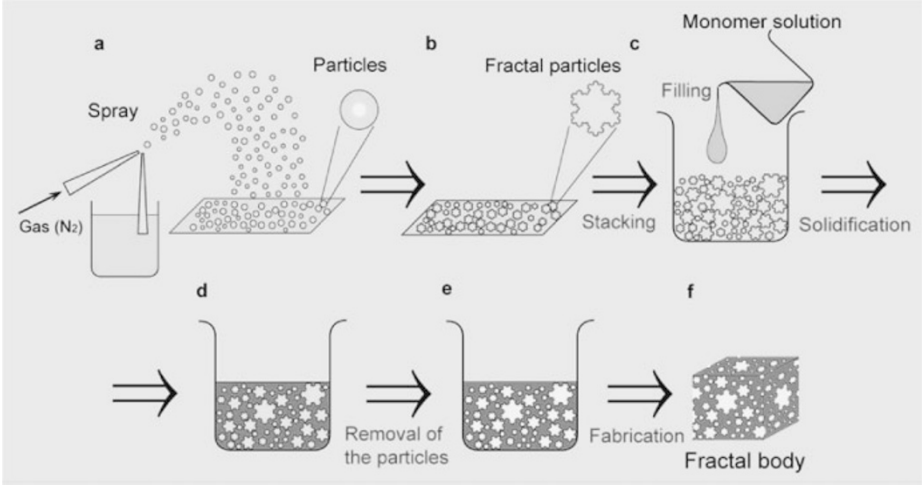

Figure 23. Schematic representation of experimental strategy in creation of a fractal body. (a)–(b) Preparation of templates. (c) Packing and compression of templates. (c)–(d) Filling the remained space by a suitable monomer solution and its solidification. (e) Removal of templates. (f) Fractal body.

Polymer Journal

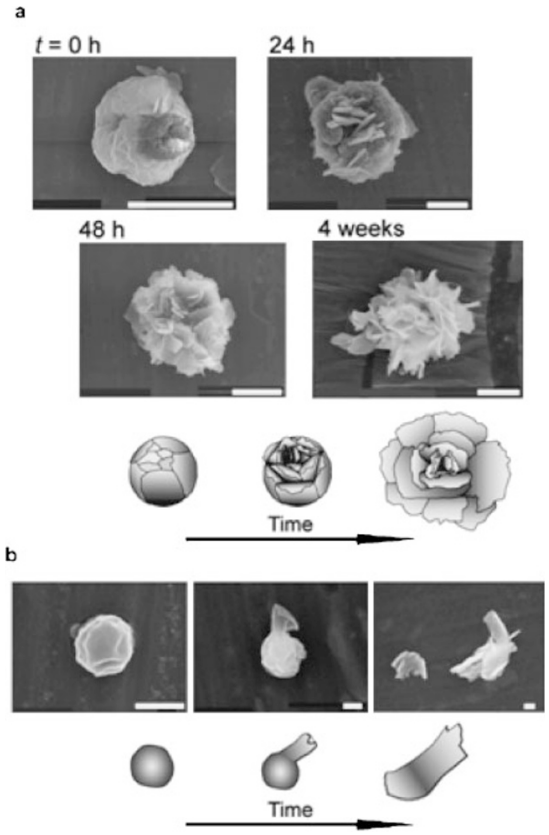

Figure 24. Spontaneous formation of flower-like fractal AKD particles (diameter ≥ 5 μm) and their schematic representations (a), and spontaneous change of smaller particles (< 5 μm) and their schematic representation (b). Scale bars: 5 μm.

same process without AKD particles was confirmed to be transparent and its density was 2.4 g cm^{-3}, which is consistent with that of usual SiO_2 glass. Therefore, the volume fraction f for each sample was 0.15 (silica: 15%, air: 85%), 0.08 (silica: 8%, air: 92%) and 0.04 (silica 4%, air 96%) at $r_c = 1$, 2 and 3, respectively.[38]

Next, we observed cross sections of the prepared porous silica to determine the fractal dimension of the cross section D_{cs} by the box-counting method. Figure 25(a) and 25(b) show a schematic representation of FIB technique and a cube (size ≈ 70 μm) of porous silica at $r_c = 1$ fabricated by a FIB, respectively.[38] Wide distributions of shape and size of pores were observed on the faces. In the FIB fabrication, it was easy to obtain clear cross section on a mass of porous silica.

Figure 26 shows typical SEM images of the cross-sectional porous silica at $r_c = 1$ at different magnification over *ca.* two decades and their corresponding pictorial images. Similar SEM results to Figure 26 were obtained also for the samples at $r_c = 2$ and 3. We determined D_{cs} by the box-counting method from the above pictorial images. Figure 27 shows the plots of $\log N(r)$ *vs.* $\log r$ obtained by the box-counting method for each sample.[38] There are two inflection points in each plot. For example, the plot for the sample at $r_c = 1$ is inflected at ~50 nm and ~30 μm. D_{cs} was determined to be 1.87 between

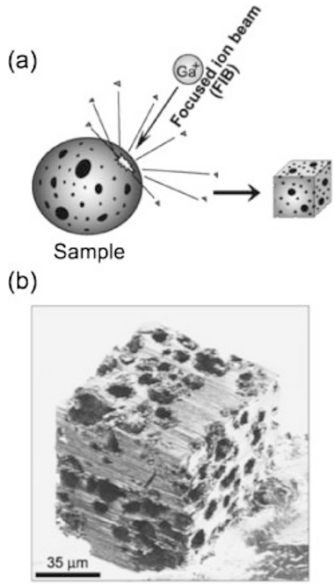

Figure 25. Schematic representation of a FIB (a), and typical SEM image of a cube of porous silica prepared at $r_c = 1$ (b).

the two points, whereas $D_{cs} \sim 2$ below 50 nm and above 30 μm. From the plots of $\log N(r)$ *vs.* $\log r$, one can see that almost three decades between $l \sim 50$ nm and $L \sim 30$ μm in pore size are in the fractal (self-similar) nature, where l and L corresponds to the sizes of the thickness of the flake crystal and the maximum particle size of the template, respectively. The values of the obtained D_{cs} at $r_c = 1$, 2 and 3 were 1.87, 1.84 and 1.80, respectively.

It is possible to discuss the fractal geometry based on volume fraction because it reflects fractal geometry such as fractal dimension, number of hierarchical structure and cutoffs. Let's consider volume fraction f_n at the n-th generation based on the model in Figure 22. The sponge of $n = 1$ consists of 20 identical cubes in the total volume of 27 cubes and then $f_1 = (20/27)$. Next, the sponge of $n = 2$ is constituted of 20 units of the volume-reduced sponge of $n = 1$ and then $f_2 = (20/27)^2$. Therefore, $f_n = (20/27)^n$ at the n-th generation. If one can determine n, then theoretical f_n can be obtained. How can we evaluate n from the experimental results? The n is correlated with the ratio of minimum pore size to maximum one as follows. Assuming the original pore size to be a at $n = 1$ and the size reduction ratio by one generation to be r_{size}, the size becomes ar_{size} at $n = 2$ and $ar_{size}{}^2$ at $n = 3$. Therefore, the pore size at the n-th generation is represented as $ar_{size}{}^{n-1}$, where the minimum size r_{min} and maximum one r_{max} are $ar_{size}{}^{n-1}$ and a, respectively. The ratio of r_{min} to r_{max} is

$$r_{min}/r_{max} = r_{size}^{n-1}, \tag{9}$$

where r_{min} and r_{max} are equal to l and L, respectively. For $r_c = 1$, D_{cs} was close to Menger's sponge and $r_{size} \sim 1/3$. Consequently, $(1/3)^{n-1} \sim 10^{-3}$, then n and f are determined to be 7 and $(20/27)^7 \sim 0.12$, respectively, it is in good agreement with the experimental result of $f(0.15)$ within the experimental error.

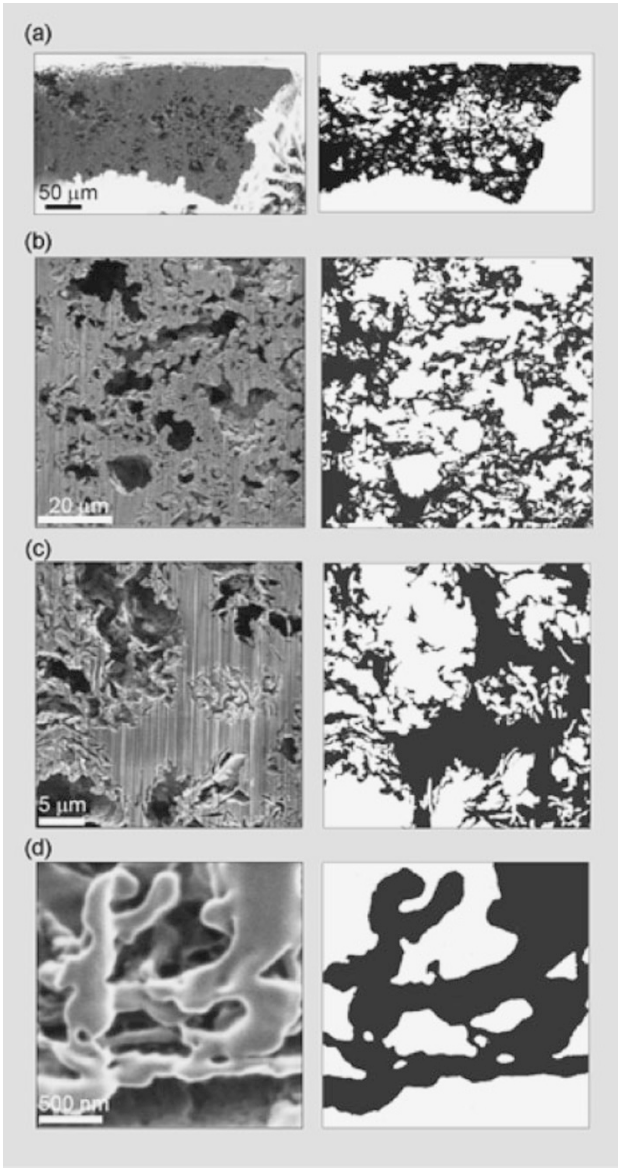

Figure 26. Typical SEM images of the cross-sectional porous silica of $r_c = 1$ (left) and their pictorial images (right) at different magnification.

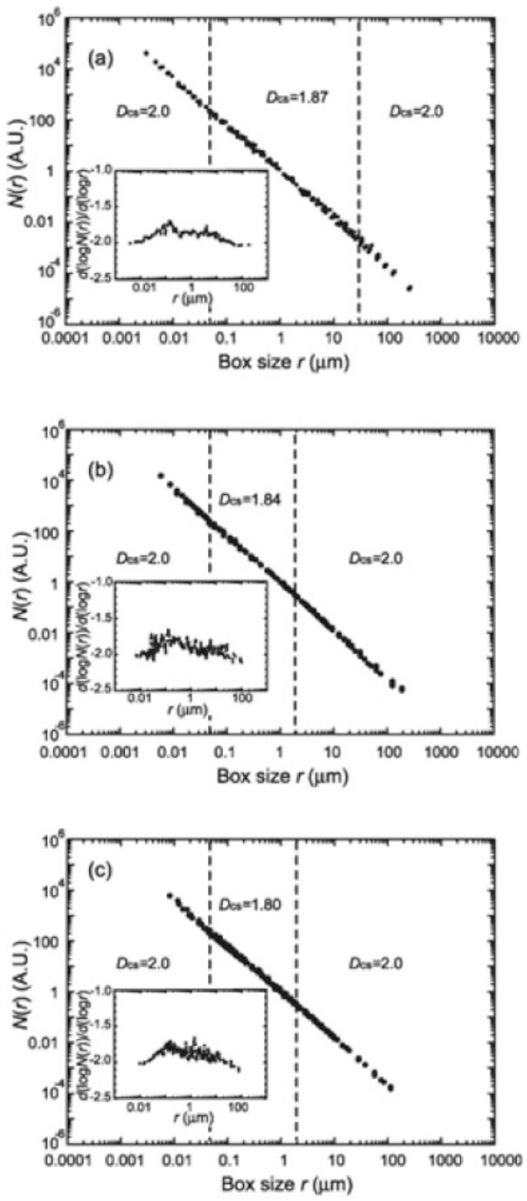

Figure 27. The plots of $\log N(r)$ *vs.* $\log r$ in the cross-sections for the fractal bodies at $r_c = 1$ (a), 2 (b) and 3 (c). The insets show the plots of $d(\log N(r))/d(\log r)$ *vs.* $\log r$.

We have now just succeeded in making some fractal bodies, and do not know yet any interesting properties and/or useful functions of these unique materials. The research to find out such properties and functions is now in progress.

Received: February 20, 2008
Accepted: March 27, 2008
Published: May 28, 2008

REFERENCES

1. B. B. Mandelbrot, "The Fractal Geometry of Nature," Freeman, San Francisco, 1982.
2. "Fractal Approach to Heterogeneous Chemistry," D. Avnir, Ed., John Wiley and Sons, Inc., New York, 1989.
3. T. Onda, S. Shibuichi, N. Satoh, and K. Tsujii, *Langmuir*, **12**, 2125 (1996).
4. S. Shibuichi, T. Onda, N. Satoh, and K. Tsujii, *J. Phys. Chem.*, **100**, 19512 (1996).
5. K. Tsujii, T. Yamamoto, T. Onda, and S. Shibuichi, *Angew. Chem., Int. Ed.*, **36**, 1011 (1997).
6. S. Shibuichi, T. Yamamoto, T. Onda, and K. Tsujii, *J. Colloid Interface Sci.*, **208**, 287 (1998).
7. A. W. Adamson and A. P. Gast, "Physical Chemistry of Surfaces," 6th ed., John Wiley & Sons, Inc., New York, 1997, p. 353.
8. R. W. Wenzel, *Ind. Eng. Chem. Res.*, **28**, 988 (1936).
9. R. D. Hazlett, *J. Colloid Interface Sci.*, **137**, 527 (1990).
10. A. B. D. Cassie and S. Baxter, *Trans, Faraday Soc.*, **40**, 546 (1944).
11. T. Vicsek, "Fractal Growth Phenomena," World Scientific Publishing, Singapore, 1989, Chapter 2.
12. W. Fang, H. Mayama, and K. Tsujii, *J. Phys. Chem. B*, **111**, 564 (2007).
13. R. E. Timms, *Prog. Lipid Res.*, **23**, 1 (1984).

14. S. Shibuichi, T. Onda, N. Satoh, and K. Tsujii, *J. Jpn. Oil. Chem. Soc.*, **46**, 649 (1997).
15. E. Laine, P. Auramo, and P. Kahela, *Int. J. Pharm.*, **43**, 241 (1988).
16. M. Kellens, W. Meeussen, R. Gehrke, and H. Reynaers, *Chem. Phys. Lipids*, **58**, 131 (1991).
17. V. Hongisto, V. Lehto, and E. Laine, *Thermochim. Acta*, **276**, 229 (1996).
18. K. Sato, S. Ueno, and J. Yano, *Prog. Lipid Res.*, **38**, 91 (1999).
19. K. W. Smith, F. W. Cain, and G. J. Talbot, *J. Agric. Food Chem.*, **53**, 3031 (2005).
20. W. MacNaughtan, I. A. Farhat, C. Himawan, V. M. Starov, and A. G. F. Stapley, *J. Am. Oil Chem. Soc.*, **83**, 1 (2006).
21. W. Fang, H. Mayama, and K. Tsujii, *Colloids Surf. A*, **316**, 258 (2008).
22. T. Minami, H. Mayama, S. Nakamura, S. Yokojima, J. Shen, and K. Tsujii, *Soft Matter*, **4**, 140 (2008).
23. J. N. Israelachvili, "Intermolecular and Surface Forces," 2nd ed., Academic Press, London, 1992, p. 316.
24. A. W. Adamson and A. P. Gast, "Physical Chemistry of Surfaces," 6th ed., John Wiley & Sons, Inc., New York, 1997, p. 368.
25. A. Tuteja, W. Choi, M. Ma, J. M. Mabry, S. A. Mazzella, G. C. Rutledge, G. H. McKinley, and R. E. Cohen, *Science*, **318**, 1618 (2007).
26. K. Kurogi, H. Yan, and K. Tsujii, *Colloids Surf. A*, **317**, 592 (2008).
27. S. Asavapiriyanont, G. K. Chandler, G. A. Gunawardena, and D. Pletcher, *J. Electroanal. Chem.*, **177**, 229 (1984).
28. P. G. Pickup and R. A. Osteryoung, *J. Am. Chem. Soc.*, **106**, 2294 (1984).
29. R. E. Noftle and D. Pletcher, *J. Electroanal. Chem.*, **227**, 229 (1987).
30. M. Satoh, K. Kaneto, and K. Yoshino, *Synth. Met.*, **14**, 289 (1986).
31. "Handbook of Conjugated Polymers," T. A. Skotheim, R. L. Elsenbaumer, and J. Reynolds, Ed., Marcel Dekker, New York 1996.
32. G. Kossmehl and M. Niemitz, *Synth. Met.*, **41–43**, 1065 (1991).
33. M. Niemitz and G. Kossmehl, *Angew. Makromol. Chem.*, **185**, 147 (1991).
34. H. Yan, K. Kurogi, H. Mayama, and K. Tsujii, *Angew. Chem., Int. Ed.*, **44**, 3453 (2005).
35. K. Kurogi, H. Yan, H. Mayama, and K. Tsujii, *J. Colloid Interface Sci.*, **312**, 156 (2007).
36. H. Yan, K. Kurogi, and K. Tsujii, *Colloids Surf. A*, **292**, 27 (2007).
37. M. W. Takeda, S. Kirihara, Y. Miyamoto, K. Sakoda, and K. Honda, *Phys. Rev. Lett.* **92**, 093902 (2004).
38. H. Mayama and K. Tsujii, *J. Chem. Phys.*, **125**, 124706 (2006).
39. R. K. Iler, "The Chemistry of Silica" Wiley, New York, 1979.

Kaoru TSUJII was born in Osaka, Japan, in 1945, and graduated from the Department of Chemistry of Osaka University, Osaka, Japan in 1968. He studied physical chemistry and awarded Master of Science in 1970 and Doctor of Science in 1983 at the same university. He joined R&D Division of Kao Corporation in 1970 until 1998. During this period, he worked in Texas A&M University, USA from 1975 to 1976. He was the director of Tokyo Research Institute from 1988 to 1989, and of Kao Institute for Fundamental Research from 1990 to 1994. He moved to Japan Marine Science and Technology Center in 1998, and was a program director. He was appointed full professor of Nanotechnology Research Center, Research Institute for Electronic Science, Hokkaido University in 2003. He retired the Hokkaido University in 2008. He served as chairman of Colloid and Surface Chemistry Division, The Chemical Society of Japan from 1999 to 2001. He was awarded the Progress award for young researcher (Japan Oil Chemists' Society) in 1982, the Outstanding paper presentation award (American Oil Chemists' Society) in 1993, the Most valuable technical paper award (Association of Oil and Fat Industry, Japan) in 1998, the Divisional award of the Chemical Society of Japan in 1999, and the Mitsubishi Chemical Award (The Society of Polymer Science, Japan) in 2007.